Visualizing Ion Relaxation in the Transport of Short DNA Fragments

Stuart A. Allison,* Hua Wang,* Thomas M. Laue,# Timothy J. Wilson,# and John O. Wooll#
*Department of Chemistry, Georgia State University, Atlanta, Georgia 30303, and #Department of Biochemistry and Molecular Biology, Rudman Hall, University of New Hampshire, Durham, New Hampshire 03824-3544 USA

ABSTRACT Ion relaxation plays an important role in a wide range of phenomena involving the transport of charged biomolecules. Ion relaxation is responsible for reducing sedimentation and diffusion constants, reducing electrophoretic mobilities, increasing intrinsic viscosities, and, for biomolecules that lack a permanent electric dipole moment, provides a mechanism for orienting them in an external electric field. Recently, a numerical boundary element method was developed to solve the coupled Navier-Stokes, Poisson, and ion transport equations for a polyion modeled as a rigid body of arbitrary size, shape, and charge distribution. This method has subsequently been used to compute the electrophoretic mobilities and intrinsic viscosities of a number of model proteins and DNA fragments. The primary purpose of the present work is to examine the effect of ion relaxation on the ion density and fluid velocity fields around short DNA fragments (20 and 40 bp). Contour density as well as vector field diagrams of the various scalar and vector fields are presented and discussed at monovalent salt concentrations of 0.03 and 0.11 M. In addition, the net charge current fluxes in the vicinity of the DNA fragments at low and high salt concentrations are briefly examined and discussed.

INTRODUCTION

The ion atmosphere surrounding a charged particle, or polyion, in solution can be perturbed from its equilibrium value in a number of ways. In a sedimentation velocity experiment, where the driving force is a centrifugal force, the ion atmosphere tends to lag behind the translating charged particle (Booth, 1954). This ion relaxation, in turn, retards the motion of the polyion resulting in a larger translational friction coefficient, or smaller sedimentation constant, relative to an equivalent uncharged particle. Similarly, a dilute suspension of charged particles placed in a shear field exhibits a larger viscosity than the corresponding suspension of uncharged particles (Booth, 1950b; Sherwood, 1980; Sherwood, 1981; Allison, 1998). In this article, steady state shall refer to a polyion that translates with constant velocity in a viscous fluid due to the presence of a constant external driving force. In steady-state free solution electrophoresis, the driving force is a constant external electric field. In this case, the ion atmosphere is distorted both by the electric field and by the transport of the charged particle through the fluid (Booth, 1950a; Wiersema et al., 1966; O'Brien and White, 1978; Stigter, 1978a,b). Ion relaxation reduces the electrophoretic mobility, and this relaxation effect becomes more significant as the charge on the polyion increases. Over the last few years, boundary element (BE) methods that account for ion relaxation have been developed, and this has made it possible to estimate the free solution electrophoretic mobility of rigid model polyions of arbitrary size and charge distribution (Allison, 1996). This approach has been applied to lysozyme (Allison and et al., 1997) and short DNA fragments (Allison and Mazur, 1998). When ion relaxation is included, calculated mobilities of 20-bp DNA fragments in 0.11 M KCl agree with experimental mobilities (Laue et al., 1996) to within a few percent. For a 27-bp fragment in 0.04 M Tris acetate, calculated and experimental (Stellwagen et al., 1997) mobilities agree to within 10–15%. Furthermore, ion relaxation reduces the mobility at 0.11 M KCl by 25% relative to the predicted mobility in its absence (Allison and Mazur, 1998). A final electrooptical phenomenon worthy of mention involves orienting macroions in solution by external electric fields and monitoring this by optical birefringence or dichroism. Partial orientation occurs as a result of the interaction of the external field with the electric dipole moment of the macroion. Whether the dipole is permanent or induced can be distinguished by field reversal techniques (Tinoco and Yamaoka, 1959) or by the field strength dependence of birefringence/dichroism (Stellwagen, 1981). DNA fragments have been extensively studied by these methods (Elias and Eden, 1981; Stellwagen, 1981; Hagerman, 1981; Diekmann et al., 1982; Porschke, 1994), and the dipole is primarily, though not exclusively, induced (Elias and Eden, 1981; Stellwagen, 1981). In this example, the induced dipole moment develops as a consequence of ion relaxation (Fixman and Jagannathan, 1981). The above cases serve to illustrate that ion relaxation plays an important role in biophysics and the transport of macroions in general.

As discussed above, it is now possible to account for ion relaxation in modeling the transport of rigid macroions of arbitrary shape and charge distribution, and this approach has been used to calculate electrophoretic mobilities and intrinsic viscosities for DNA fragments and lysozyme. The purpose of the present work is to provide visual demonstration of the relaxation effect by looking at various scalar and vector fields around short DNA fragments. The present

Received for publication 9 November 1998 and in final form 5 February 1999.

Address reprint requests to Dr. Stuart Allison, Department of Chemistry, Georgia State University, University Plaza, Atlanta, GA 30303. Tel.: 404-651-1986; Fax: 404-651-3099; E-mail: chesaa@panther.gsu.edu.

0006-3495/99/05/2488/14 $2.00

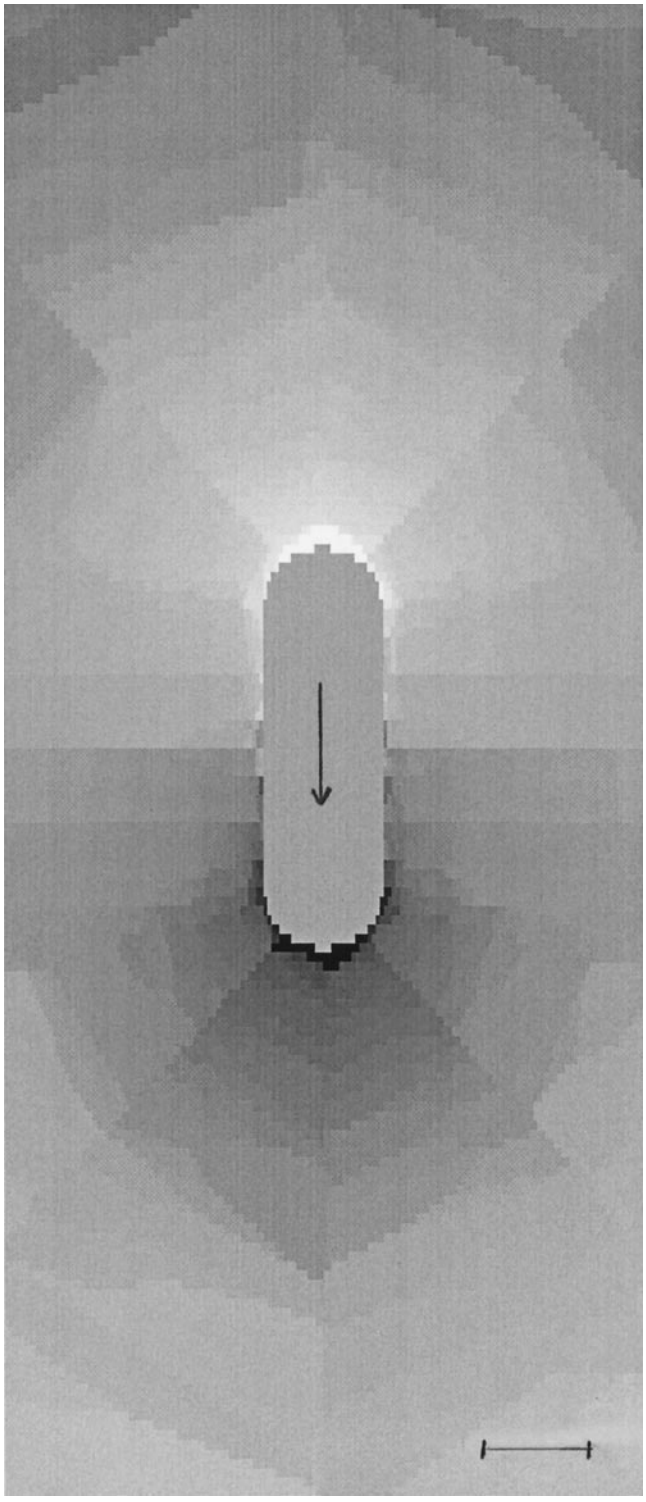

FIGURE 1 δn_+ for sedimentation of 20-bp DNA in 0.03 M KCl. The fragment is translating along the cylinder axis in the direction of the arrow. White shading corresponds to the greatest positive deviation in counterion concentration from equilibrium and black to the greatest negative deviation. Neutral gray (which also shades the fragment interior) corresponds to $\delta n_+ = 0$. The range in $\delta n_+/c_{+0}$ is $\sim\pm 9 \times 10^{-6}$. Ten different gray shadings appear in the figure that reflect this range. The bar at lower right denotes $\kappa^{-1} = 1.74$ nm.

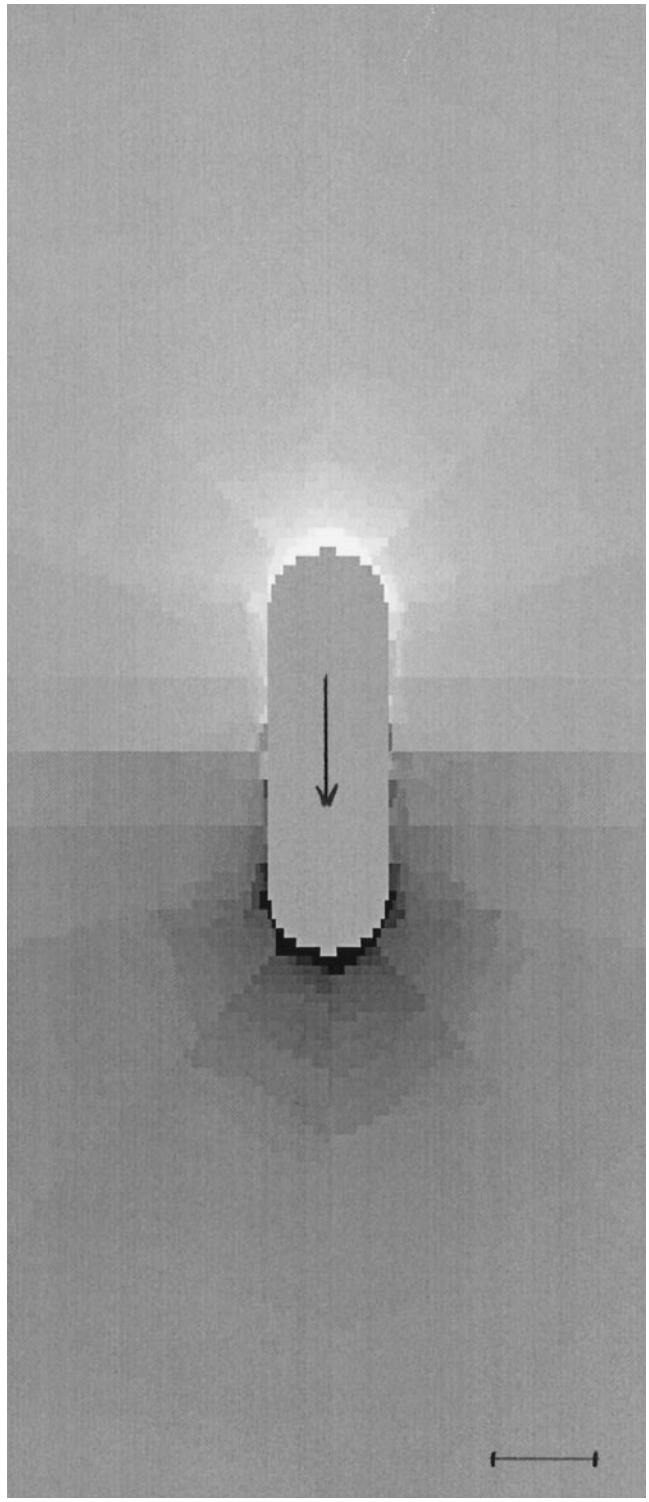

FIGURE 2 $\delta\rho$ for sedimentation of 20-bp DNA in 0.03 M KCl. The fragment is translating along the cylinder axis in the direction of the arrow. White shading corresponds to the greatest positive deviation in charge density from equilibrium and black to the greatest negative deviation. Neutral gray (which also shades the fragment interior) corresponds to $\delta\rho = 0$. The range in $\delta\rho/qc_{+0}$ is $\sim\pm 9 \times 10^{-6}$. The bar at lower right denotes $\kappa^{-1} = 1.74$ nm.

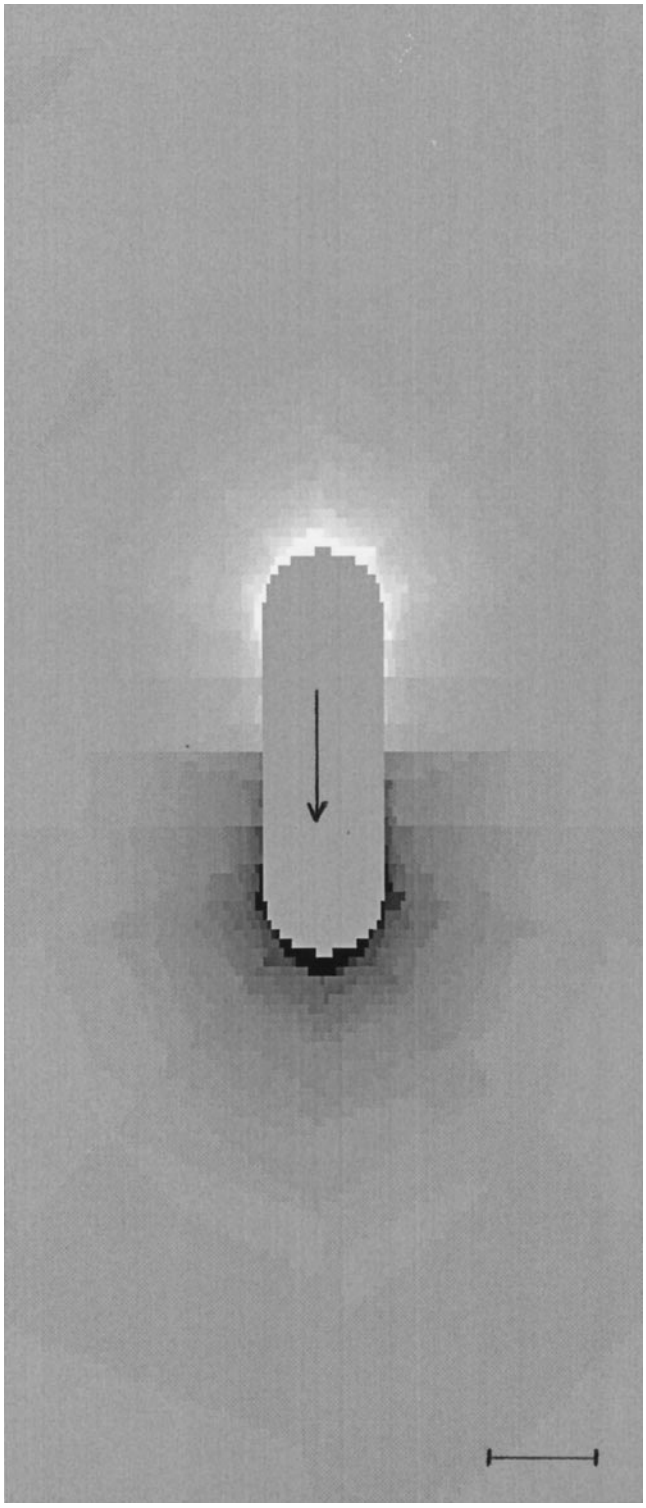

FIGURE 3 $\delta\rho$ for electrophoresis of 20-bp DNA in 0.03 M KCl. As in Fig. 2, the polyion translates in the direction of the arrow, but the driving force is a constant electric field (opposite to the flow direction). The DNA is in steady-state motion. White shading corresponds to the greatest positive deviation in charge density (from equilibrium) and black to the greatest negative deviation. Neutral gray (which also shades the fragment interior) corresponds to $\delta\rho = 0$. The range in $\delta\rho/qc_{+0}$ is $\sim\pm 3 \times 10^{-4}$. The bar at lower right denotes $\kappa^{-1} = 1.74$ nm.

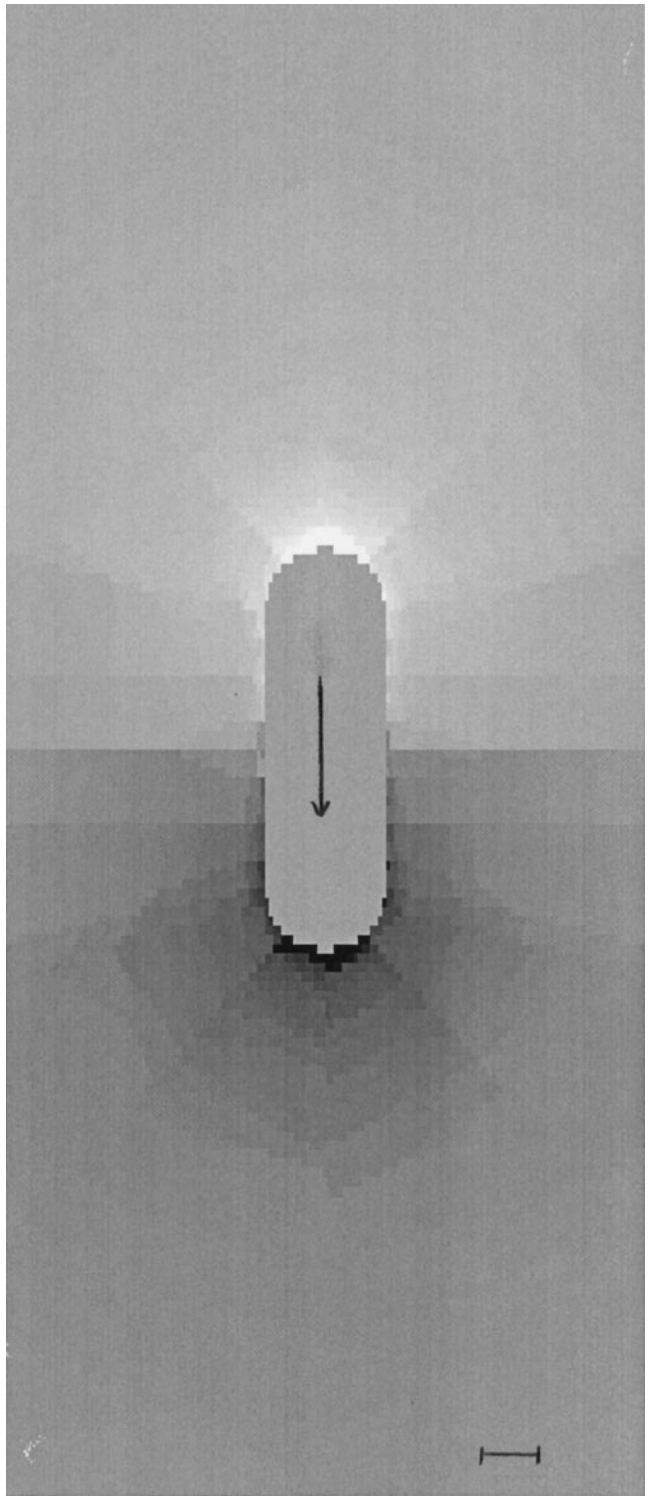

FIGURE 4 $\delta\rho$ for electrophoresis of 20-bp DNA in 0.11 M KCl. The polyion translates in the direction of the arrow, but the driving force is a constant electric field (opposite to the flow direction). The DNA is in steady-state motion. White shading corresponds to the greatest positive deviation in charge density and black to the greatest negative deviation. Neutral gray (which also shades the fragment interior) corresponds to $\delta\rho = 0$. The range in $\delta\rho/qc_{+0}$ is $\sim\pm 6 \times 10^{-5}$. The bar at lower right denotes $\kappa^{-1} = 0.91$ nm.

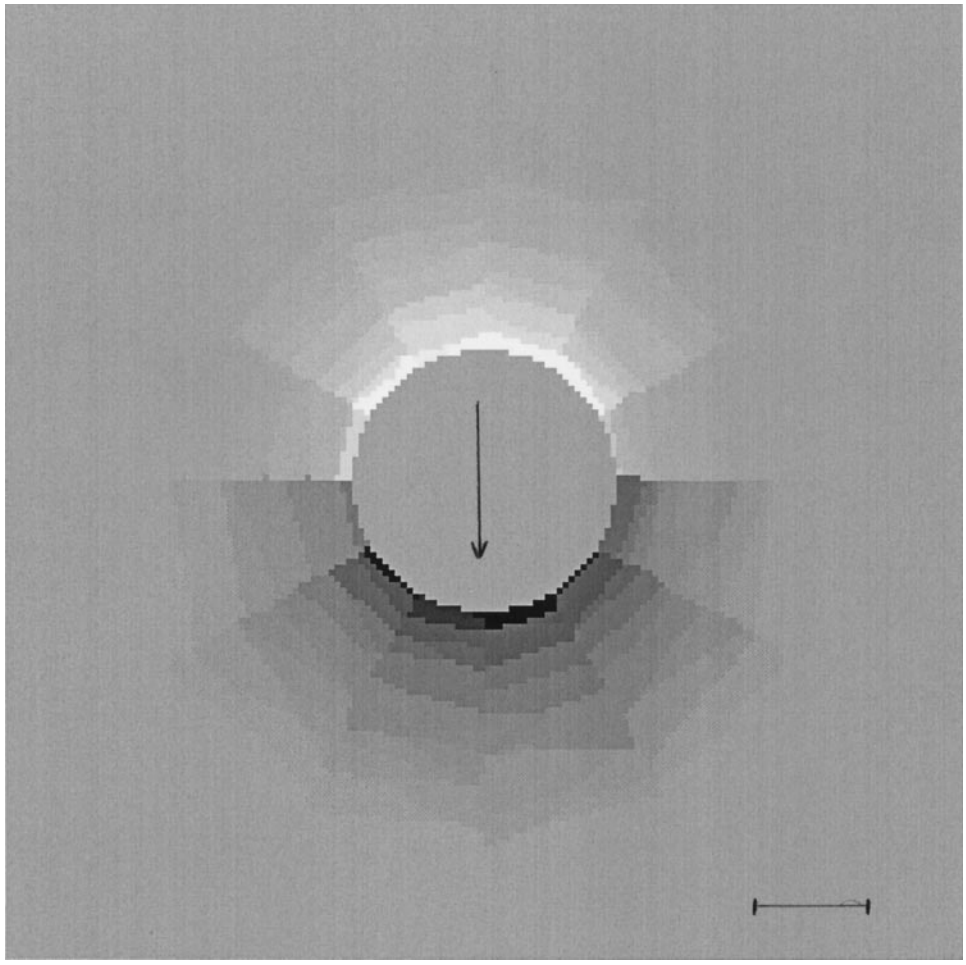

FIGURE 5 $\delta\rho$ for electrophoresis of 20-bp DNA in 0.11 M KCl. Similar to Fig. 4, but the cylinder model of DNA translates (in the direction of the arrow) in a direction perpendicular to the long axis of the polyion. In this contour density plot, one is looking down the long axis of the DNA at a plane that bisects the center of the cylinder. The polyion is in steady-state motion. White shading corresponds to the greatest positive deviation in charge density and black to the greatest negative deviation. Neutral gray (which also shades the fragment interior) corresponds to $\delta\rho = 0$. The bar at lower right denotes $\kappa^{-1} = 0.91$ nm.

study is similar to that of Stigter's 1980 paper on spherical colloid particles (Stigter, 1980). We shall focus on free solution electrophoresis, but by doing so, it is also possible to examine the sedimentation problem as well. Provided the external electric field is sufficiently weak that the electrophoretic mobility is independent of field strength, one can view electrophoresis as a superposition of two transport cases (O'Brien and White, 1978). In case 1, the polyion translates at constant velocity through a stationary fluid in the absence of an electric field. This, however, corresponds to sedimentation velocity. In case 2, the polyion is held stationary but is subjected to a constant electric field. Steady-state electrophoresis corresponds to that superposition of the two cases that results in a net force of zero acting on the polyion.

METHODS

The "primitive" model (McQuarrie, 1976) is employed in which the solvent is characterized as a continuum with a dielectric constant of 78 and a viscosity of 0.010 poise corresponding to water at 20°C. The polyion is modeled as a rigid body the surface of which is subdivided into a large number of connected triangular plates. In the present study, models of DNA fragments 20 and 40 bp in length are considered. They are modeled as capped cylinders of length (in nm) 0.34 N_{bp} (N_{bp} = number of base pairs) and diameter equal to 2 nm. As discussed previously (Allison and Mazur, 1998), these models accurately reproduce the translational and rotational diffusion constants of the actual fragments. The charge distribution is modeled as a uniform line charge extending from the origin of one hemispherical cap to the other. The total fragment charge is $-2\ N_{bp}\ q$ where q is the protonic charge. The polyion concentration is assumed to be low enough so that interactions between different polyions can be ignored.

The primitive model is also employed to represent the counterion and co-ion distributions about a single macroion. In the absence of an electric or flow field, the equilibrium electrostatic potential of mean force at position $\mathbf{r}$, $\Lambda_0(\mathbf{r})$, is related to the equilibrium local charge density $\rho_0(r)$ by the equilibrium Poisson equation:

$$\nabla \cdot (\epsilon \nabla \Lambda_0(\mathbf{r})) = -4\pi\rho_0(\mathbf{r}), \tag{1}$$

where ϵ is the local dielectric constant. In the fluid domain,

$$\rho_0(\mathbf{r}) = q \sum_\alpha z_\alpha n_{\alpha 0}(\mathbf{r}) = q \sum_\alpha z_\alpha c_{\alpha 0} e^{-\beta q z_\alpha \Lambda_0(\mathbf{r})}, \tag{2}$$

where q is the protonic charge, z_α is the valence of ion α, $n_{\alpha 0}(\mathbf{r})$ is the local concentration of ion α, $\beta = (k_B T)^{-1}$ (k_B is Boltzmann's constant and T is the absolute temperature), and $c_{\alpha 0}$ is the concentration of ion α far from the polyion. The physical significance of $\Lambda_0(\mathbf{r})$ is that if we placed a test charge q_t at position $\mathbf{r}$, then the average electrostatic potential energy of our test charge would be $q_t \Lambda_0(\mathbf{r})$ (McQuarrie, 1976). A variety of numerical methods are now available to solve the equilibrium Poisson equation for complex macromolecules (Zhou, 1994; Holst and Saied, 1995).

When a polyion is subjected to a perturbing electric and/or flow field, the mobile ion distribution is distorted from its equilibrium value, and this distortion is called ion relaxation. It shall be assumed that the perturbation

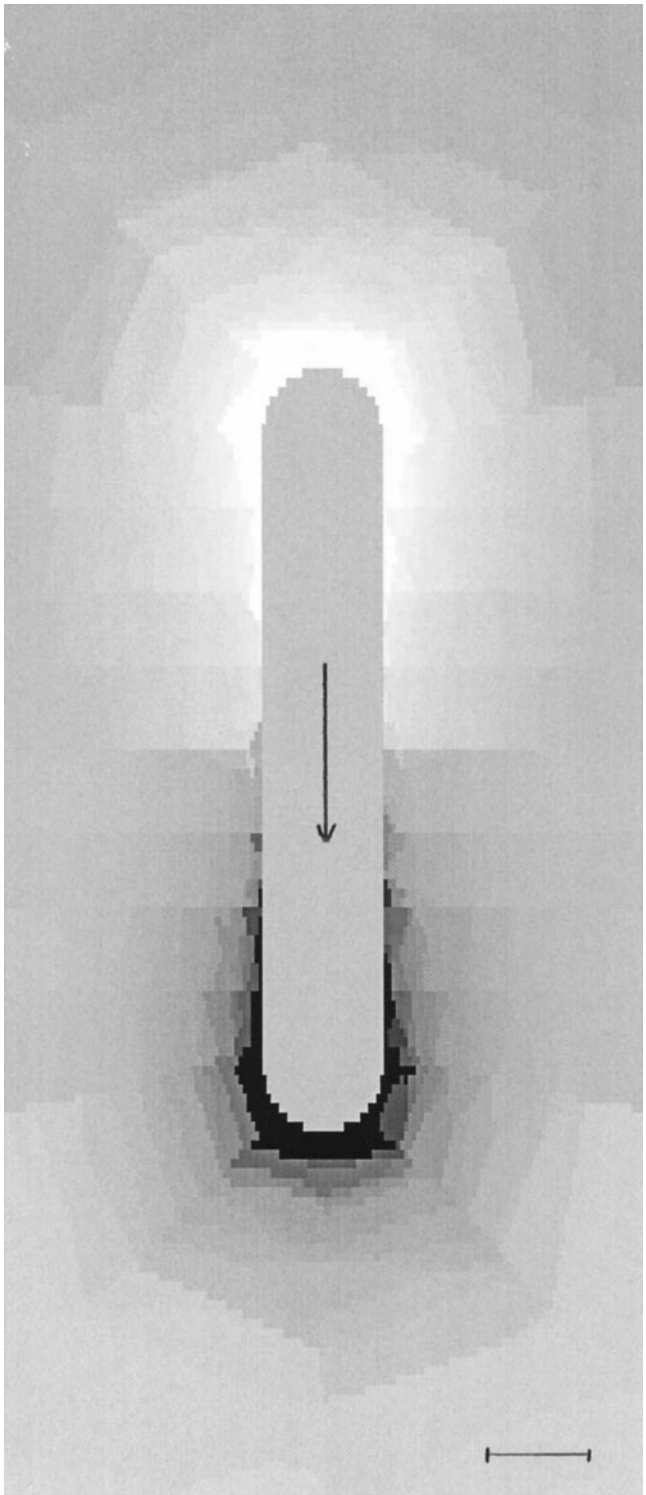

FIGURE 6 $\delta\rho$ for electrophoresis of 40-bp DNA in 0.03 M KCl. The polyion translates in the direction of the arrow along the long axis of the cylinder, but the driving force is a constant electric field (opposite to the flow direction). The DNA is in steady-state motion. White shading corresponds to the greatest positive deviation in charge density and black to the greatest negative deviation. Neutral gray (which also shades the fragment interior) corresponds to $\delta\rho = 0$. The bar at lower right denotes $\kappa^{-1} = 1.74$ nm.

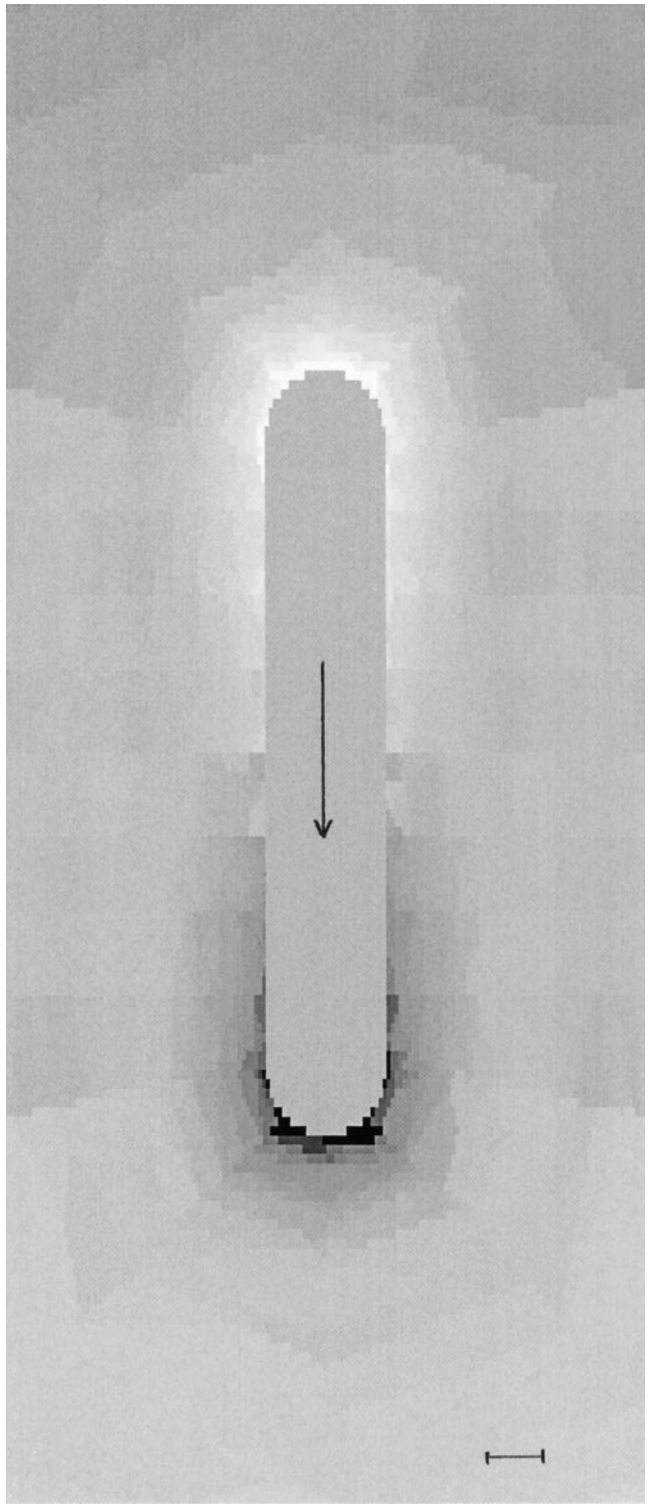

FIGURE 7 $\delta\rho$ for electrophoresis of 40-bp DNA in 0.11 M KCl. The polyion translates in the direction of the arrow, but the driving force is a constant electric field (opposite to the flow direction). The DNA is in steady-state motion. White shading corresponds to the greatest positive deviation in charge density and black to the greatest negative deviation. Neutral gray (which also shades the fragment interior) corresponds to $\delta\rho = 0$. The bar at lower right denotes $\kappa^{-1} = 0.91$ nm.

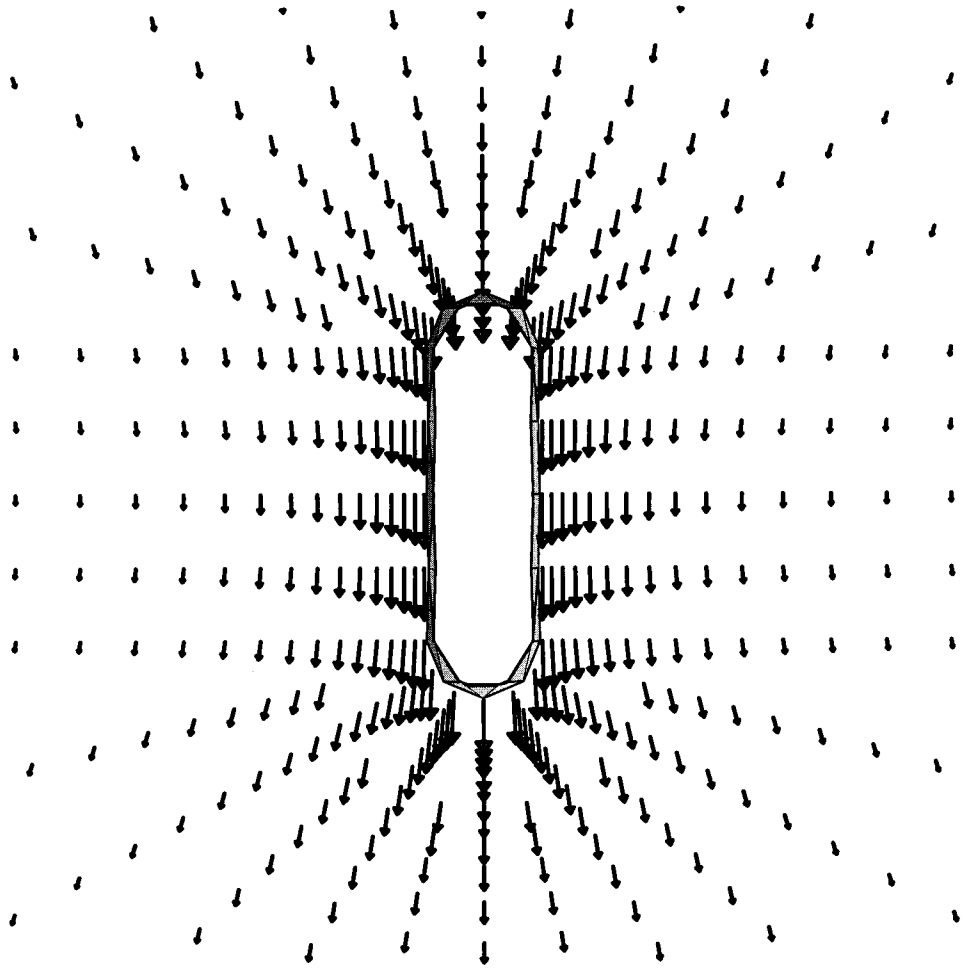

FIGURE 8 Stokes velocity field for 20-bp DNA. Fluid velocity field of an uncharged, or unrelaxed model translating parallel to the cylinder axis. Portions of the rigid model have been cut away to display the flow pattern more clearly. The structure translates at constant velocity in a fluid that is otherwise at rest.

is sufficiently weak so that only terms linear in the perturbing field(s) need to be accounted for. Including ion relaxation at the level of the primitive model requires solution of the linearized Navier-Stokes (for solvent flow), Poisson (for charge/ion distributions), and ion transport equations. It should be emphasized that these equations are coupled and must be solved simultaneously. This can be achieved in general by an iterative boundary element procedure, which is described in detail elsewhere (Allison, 1996). In the present work, we shall concentrate on only a few key features of the method in an attempt to keep the mathematics to a minimum. Let $\mathbf{j}_\alpha(\mathbf{r})$ denote the average local current density (in ions per second per unit area) in some convenient frame of reference. It can be written as the sum of convective, diffusive, and "direct force" currents:

$$\mathbf{j}_\alpha(\mathbf{r}) = n_\alpha(\mathbf{r})\mathbf{v}(\mathbf{r}) - D_\alpha \nabla n_\alpha(\mathbf{r}) + \beta n_\alpha(\mathbf{r}) D_\alpha \mathbf{f}_\alpha(\mathbf{r}), \quad (3)$$

where $n_\alpha(\mathbf{r})$ is the nonequilibrium ion concentration, $\mathbf{v}(\mathbf{r})$ is the local fluid velocity, D_α is the diffusion constant of an α-ion, and $\mathbf{f}_\alpha(\mathbf{r})$ is the local force on an α-ion. Consider the simple example of a polyion in equilibrium so that, by definition, we have no average current or fluid flow. Then Eq. 3 reduces to

$$\nabla n_{\alpha 0}(\mathbf{r}) = \beta n_{\alpha 0}(\mathbf{r})\, \mathbf{f}_{\alpha 0}(\mathbf{r}) \quad (4)$$

The equilibrium distribution of ion α about the polyion can be viewed as a dynamic equilibrium where a direct force current (which, for example, drives counterions toward the polyion surface) is balanced by an opposing diffusive current. From Eqs. 2 and 4, it is easy to deduce that $\mathbf{f}_{\alpha 0} = -qz_\alpha \nabla \Lambda_0$. At equilibrium, the force on an α-ion is its charge (qz_α) times the local electric field ($-\nabla\Lambda_0$) produced by the polyion and its ion atmosphere. When an external electric or flow field is present, however, the situation becomes more complicated. In what follows, we shall explore how a perturbing electric/flow field alters the ion distribution, fluid flow, and ion currents around the DNA fragments.

As mentioned previously, we shall restrict ourselves to short fragments in a water plus simple salt solution at 20°C. The simple salt is chosen to be KCl and the diffusion constants (D_α in Eq. 3) of K^+ and Cl^- are estimated from limiting molar conductivities (Allison and Mazur, 1998). The hydrodynamic radii of the K^+ and Cl^- ions are calculated to be 0.1242 nm.

Scalar and vector fields are first created using software of our own making. The commercial program Mathematica is then used in preparing the figures. The first seven figures are two-dimensional contour diagrams constructed through the command "ListDensityPlot". The remaining figures represent the merging of three-dimensional solid objects and the projection of a three-dimensional vector field onto a plane. The vector fields are constructed through the "ListPlotVectorField3D" command.

RESULTS AND DISCUSSION

Perturbed ion densities

When a DNA fragment or some other polyion is placed in a centrifugal (sedimentation) or electric (electrophoresis) field, the ion atmosphere is distorted from its equilibrium value. At sufficiently low centrifugal or (external) electric field strengths, the extent of distortion, or ion relaxation, varies linearly with the strength of the imposed field and vanishes at zero field strength. Consider first a 20-bp DNA

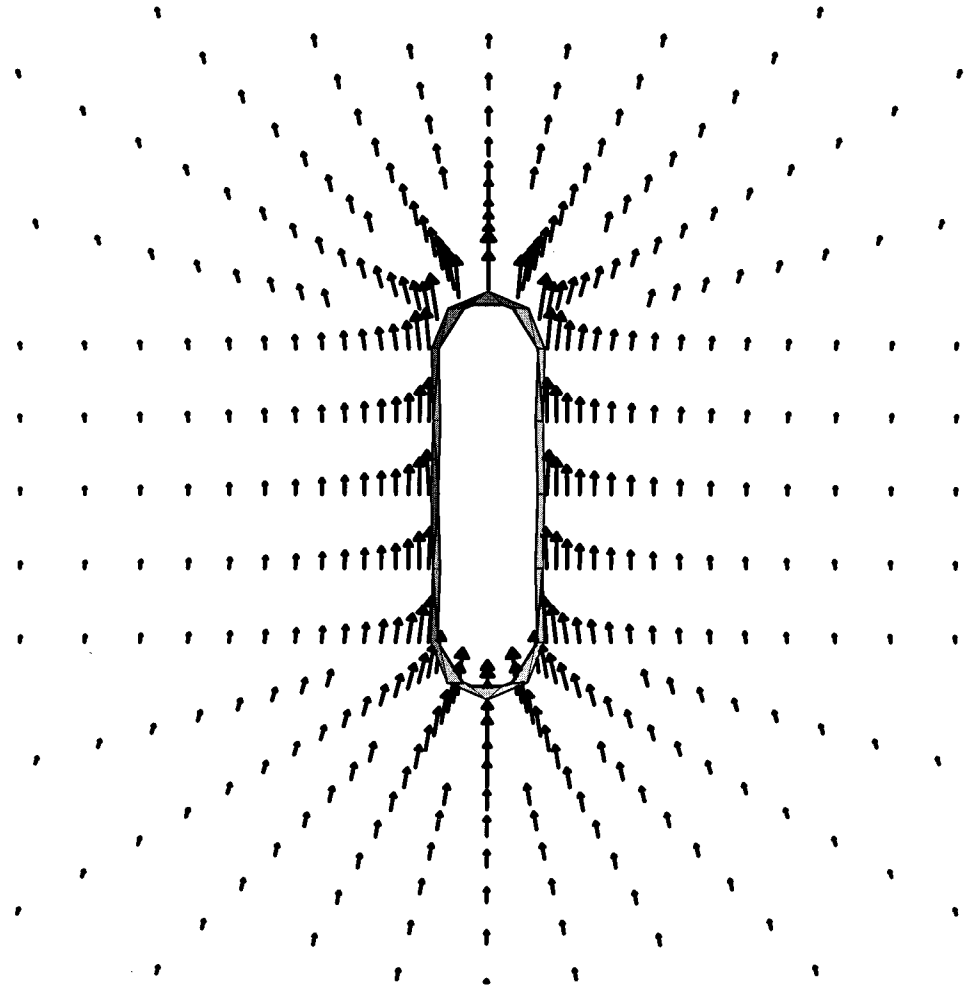

FIGURE 9 Relaxation field for sedimentation of 20-bp DNA in 0.03 M KCl. The relaxation field is defined $\delta\mathbf{v} = \mathbf{v} - \mathbf{v}_0$ where $\mathbf{v}$ is the velocity field in the presence of ion relaxation and $\mathbf{v}_0$ is the velocity field in the absence of ion relaxation. In both cases, the centrifugal force on the particles is the same and both v and $\mathbf{v}_0$ are directed toward the bottom of the figure. The relative magnitude of the vectors at the polyion surface are the same as in Fig. 8; however, the absolute value of the surface vectors in this figure are 6.4% as large as those in Fig. 8.

fragment in 0.03 M KCl at 20°C translating at steady state in a direction parallel to the cylinder axis at a velocity of 5.00×10^{-4} cm/s in response to a centrifugal force. If the fragment was in a centrifuge cell located 6.5 cm from the axis of rotation, a spin rate of approximately 2000 rpm would be necessary to achieve this velocity. Under these conditions, a plot of the counterion density $n_+(\mathbf{r})$ versus position $\mathbf{r}$ would be virtually identical to a plot of the corresponding equilibrium counterion density $n_{+0}(\mathbf{r})$. Shown in Fig. 1 is the difference plot in the counterion density, $\delta n_+ = n_+ - n_{+0}$. The DNA is translating in the direction of the arrow and white/black shades correspond to maximal excesses/deficiencies of counterions, respectively. A neutral shade of gray corresponds to $\delta n_+ = 0$ and is also used to represent the DNA interior for reference. It is seen that the greatest deficiency occurs at the leading edge of the polyion (toward the bottom of the figure) and the greatest excess is immediately behind it. At equilibrium, DNA is surrounded by an atmosphere of predominantly positive ions. As it moves, however, the front end continually enters regions of the fluid in which the positive ion concentration falls below this equilibrium value, and this accounts for the deficiency in front of the polyion. A complementary argument can explain the excess of counterions behind. In a reference frame that moves with the polyion, a steady-state distribution of mobile ions prevails, which reflects a balance of ion flow due to convection, diffusion (against a concentration gradient), and direct forces as summarized by Eq. 3. We shall return to this point later. From Fig. 1, δn_+ is seen to be dipolar in character and falls off gradually with distance. The relative difference in charge density, $\delta\rho = \rho - \rho_0$, is shown in Fig. 2 where $\rho = q(n_+ - n_-)$. All quantities have been scaled to give relative extrema that are about the same in the two figures. Although similar, it is seen that the charge density approaches the equilibrium value more quickly with distance from the polyion surface than the counterion density. The co-ion atmosphere also contributes to ion relaxation, particularly at intermediate distances from the polyion surface. Fig. 3 is similar to Fig. 2 (a contour plot of $\delta\rho$) except that the driving force is now an electric field directed opposite the polyion flow direction and is chosen sufficiently strong (1 V/cm) so that the polyion translates at the same velocity as in Figs. 1 and 2. It is clear on comparing Figs. 2 and 3 that the perturbed steady-state charge densities are very similar regardless of the nature of the driving force. It should be emphasized that the driving force in Figs. 2 and 3 are not identical in magnitude, but the steady-state velocities are.

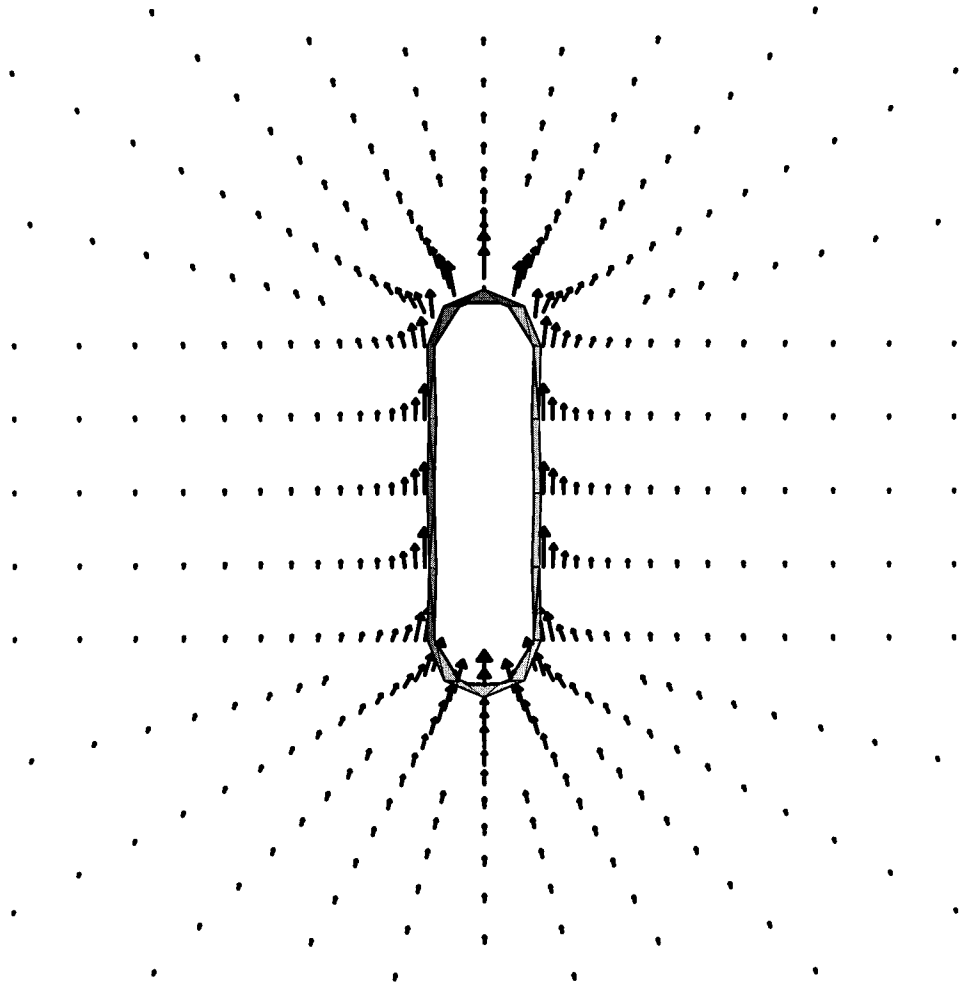

FIGURE 10 Relaxation field for sedimentation of 20-bp DNA in 0.11 M KCl. Similar to Fig. 9, but at the higher salt concentration. The relative magnitude of the vectors at the polyion surface are the same as in Fig. 8; however, the absolute value of the surface vectors in this figure are 2.8% as large as those in Fig. 8.

The contour plots shown in the first three figures come from BE calculations of model polyions made up of 144 triangular plates, and what is being plotted is a two-dimensional cut in a plane that includes the cylinder axis. As the charge distribution has been approximated by a line charge, the scalar and vector fields considered in this work should be axially symmetric to a good approximation provided the external flow/electric field is collinear with the cylinder axis. Careful inspection of these density plots show that they are not entirely symmetrical about the rod axis as they should be. This is due to noise in the computations. The similarity between ion relaxation in sedimentation (Fig. 2) and electrophoresis (Fig. 3) is expected, in part at least, because both scalar fields represent solutions of the same coupled equations, but subject to different boundary conditions. Also, Onsager relations have been derived that relate the two processes of electrophoresis and sedimentation (de Groot et al., 1952), and these have been partially confirmed (Stigter, 1980). However, it is not true that $u/u_0 = \mu/\mu_0$ where u and u_0 are the (magnitudes of the) polyion sedimentation velocities in the presence and absence of ion relaxation subject to the same centrifugal force, whereas μ and μ_0 are the electrophoretic mobilities in the presence and absence of ion relaxation but subject to the same external electric field strength. From calculations on a 144-plate model (20-bp DNA at 20°C at 0.03 M KCl and the polyion translating end-on as shown in Figs. 1–3), $u/u_0 = 0.937$ and $\mu_{\|}/\mu_{\|0} = 0.720$. These results are qualitatively consistent with the predictions for sedimentation (Booth, 1954) and electrophoresis (Booth, 1950a) of charged spheres. The orientationally averaged electrophoretic mobility predicted by the model is -4.05×10^{-4} cm^2/V s, and the experimental value under very similar salt conditions is -3.71×10^{-4} cm^2/V s (Wooll, 1994). Closer agreement between model calculations and experiment can be achieved by doing a series of calculations on models with varying number of platelets and extrapolating to the limit of infinite plate number (Allison and Mazur, 1998).

It should be emphasized that the magnitude of the ion relaxation seen in Figs. 1–3 is directly proportional to the magnitude of the polyion velocity (u), or external electric field (e). In Fig. 1 where $u = 5 \times 10^{-4}$ cm/s, the range in $\delta n_+/c_{+0}$ (c_{+0} equals the counterion concentration far from the polyion) is $\sim \pm 9 \times 10^{-6}$. The range seen in Fig. 2 is approximately the same as this as the perturbation of greatest magnitude occurs near the polyion surface where the co-ion concentration is very small. In Fig. 3, the polyion translates at the same velocity as in Fig. 2 but is also

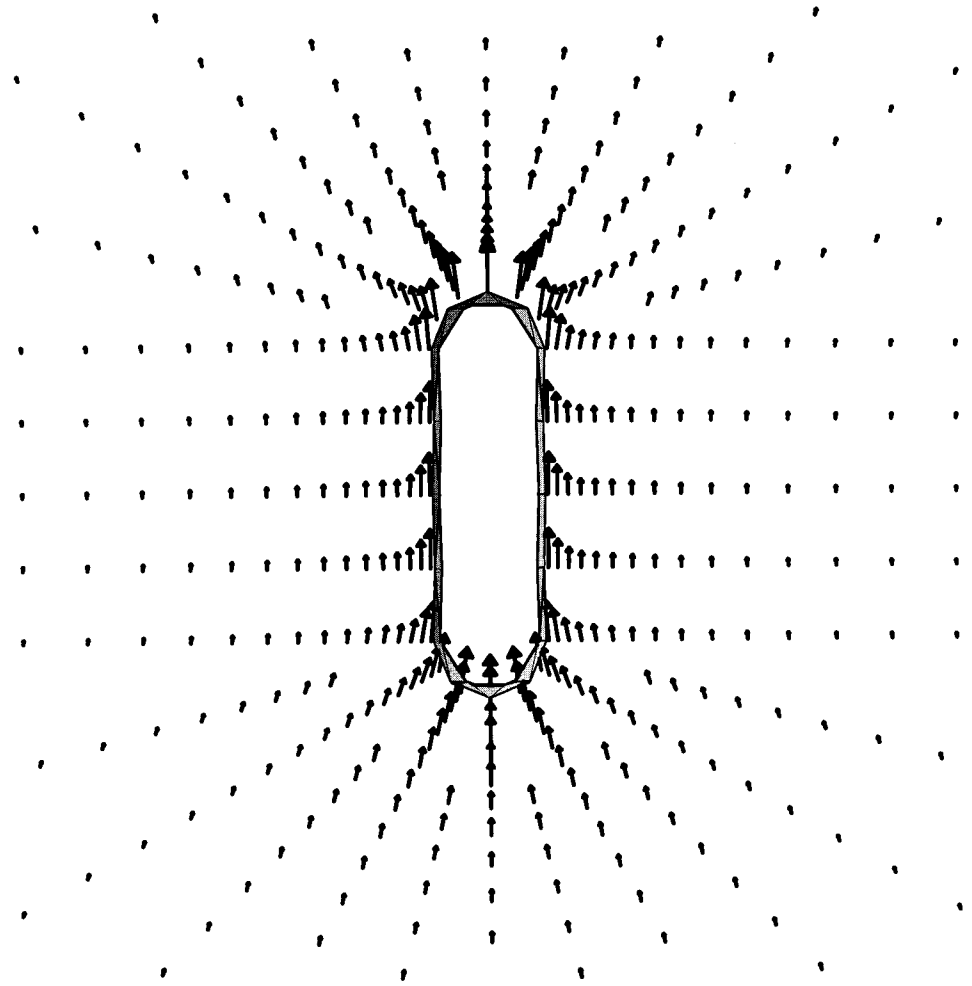

FIGURE 11 Relaxation field for electrophoresis of 20-bp DNA in 0.03 M KCl. See the caption of Fig. 9 or the text for the definition of the relaxation field. The electric field is the same in both the relaxed and unrelaxed cases and is directed upward, in the direction of $\delta\mathbf{v}$ at the model surface. The relative magnitude of the vectors at the polyion surface are the same as in Fig. 8; however, the absolute value of the surface vectors in this figure are 28% as large as those in Fig. 8.

subjected to an e-field of 1 V/cm in a direction opposing the flow direction of the polyion, and this corresponds to steady-state electrophoresis. The range in $\delta\rho/qc_{+0}$ in this case is $\sim\pm 3 \times 10^{-4}$, which, in terms of absolute magnitude, is substantially larger than the relaxation effect seen in the case of sedimentation. The fact that Figs. 2 and 3 appear very similar is due to the much narrower spacings of the contours in Fig. 2 relative to Fig. 3. Fig. 4 is similar to Fig. 3, but the KCl concentration has been increased from 0.03 to 0.11 M. The close similarity between the perturbed charge densities seen in these two figures shows that the relative ion relaxation effect is similar at the two salt concentrations for fragments of this length. However, the range in $\delta\rho/qc_{+0}$ at 0.11 M is $\sim\pm 6 \times 10^{-5}$, which is 5 times smaller than the range seen at 0.03 M. Thus, although the relative relaxation effect does not vary strongly with salt concentration, the absolute relaxation effect does and decreases with increasing salt concentration. A curious feature of electrophoresis at these two salt concentrations is that the absolute range in $\delta\rho$ is approximately the same.

In addition to contour density plots of DNA translating parallel to the cylinder axis, similar plots for DNA translating perpendicular to the cylinder axis exhibit dipolar character similar to what is seen in Figs. 1–4 when the contour plane bisects the midpoint of the cylinder. Fig. 5 shows an example of this for the electrophoresis of 20-bp DNA at 0.11 M KCl. Figs. 6 and 7 show $\delta\rho$ for 40-bp DNA at 0.03 and 0.11 M KCl, respectively. The fragments are undergoing steady-state electrophoresis in an external field of 1 V/cm directed parallel to the axis of the cylinder. Arrows at the center of the polyion indicate the direction of polyion flow. The magnitude of the drift velocities are 5.58 (0.03 M) and 5.09×10^{-4} cm/s (0.11 M), respectively. Somewhat different contour shadings/spacings are used in the 40-bp plots compared with the 20-bp plots to emphasize the differences at the two salt concentrations. Similar to the 20-bp plots, Figs. 6 and 7 show that ion relaxation is largely dipolar in character with a nodal plane ($\delta\rho = 0$) that bisects the center of the cylinder and is perpendicular to the cylinder axis. It is interesting to note from Fig. 6 that ion relaxation is not confined to the very ends of the fragment, but extends quite far along the chain from the ends. Keep in mind that the cylinder diameter is 2 nm and the reciprocal of the Debye-Huckel screening length, κ^{-1}, equals 1.74 nm and 0.91 nm at 0.03 M and 0.11 M KCl, respectively. Qualitatively, it would appear that ion relaxation is significant at distances up to several κ^{-1} from the ends of the fragment in steady-state electrophoresis.

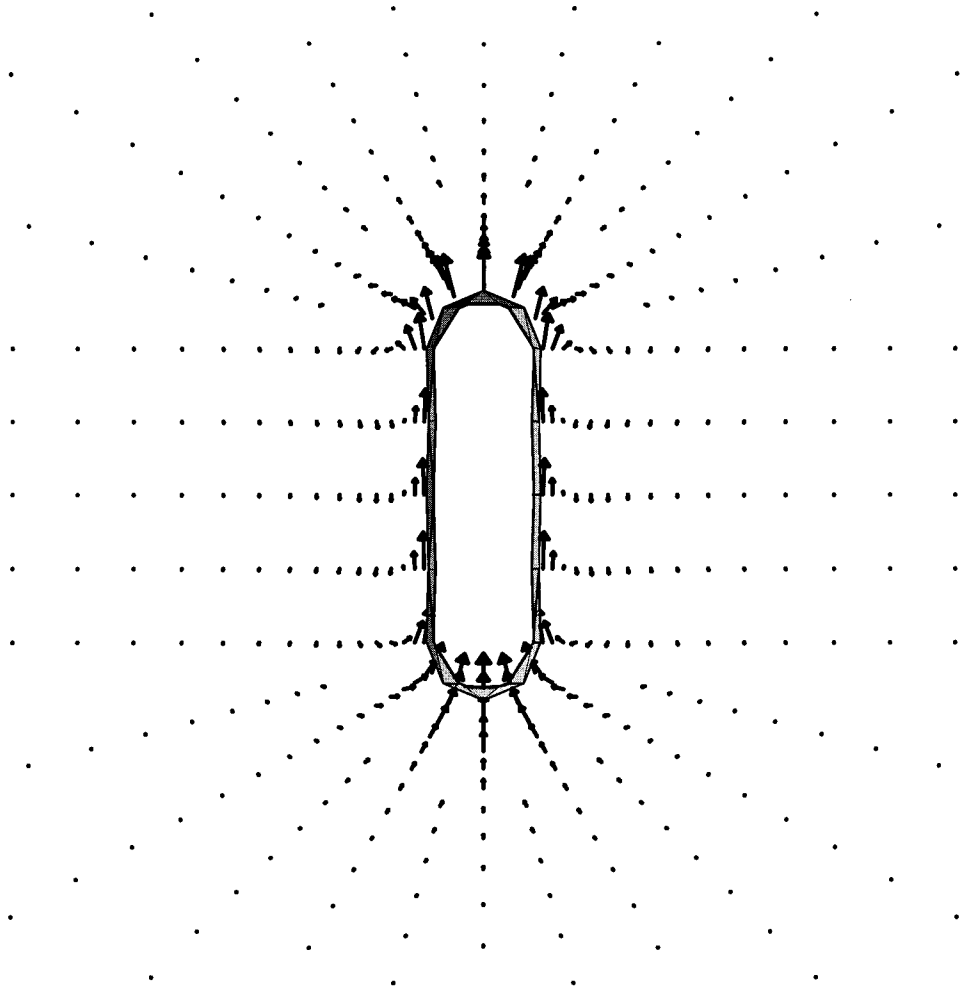

FIGURE 12 Relaxation field for electrophoresis of 20-bp DNA in 0.11 M KCl. Similar to Fig. 11, but at the higher salt concentration. The relative magnitude of the vectors at the polyion surface are the same as in Fig. 8; however, the absolute value of the surface vectors in this figure are 18% as large as those in Fig. 8.

At the same ambient salt concentration, the absolute range in $\delta\rho$ for the electrophoresis of DNA translating parallel to the cylinder axis for the 40-bp fragment is approximately the same as the 20-bp fragment. This does not necessarily imply that the induced electric dipole moment for a rod translating parallel to its axis varies linearly with length as ion relaxation effects are evidently diffuse in character and not confined to the very ends of the rod. At the present time, we are investigating the induced electric dipole moment of DNA fragments and the related problem of their electric polarizability (Fixman and Jagannathan, 1981). The extended nature of the perturbed ion densities seen in these figures does raise concern about how long range end effects are in transport properties such as the electrophoretic mobility of short DNA fragments. For a rod translating parallel to its axis in an external field, it has been argued that end effects on the electrophoretic mobility should become negligible in the limit of a very long rod (Stigter, 1978b). For DNA modeled as a rod in 0.11 M KCl and translating parallel to the rod axis, BE calculations have shown that ion relaxation reduces electrophoretic mobility by approximately 32%, 25%, and 20% for 20-bp, 40-bp, and 60-bp fragments, respectively (Allison and Mazur, 1998). Thus, end effects may very well become negligible for very long rods as proposed by Stigter, but their contribution to parallel electrophoresis appears to be quite long range.

Velocity fields

In addition to the perturbed ion and charge density plots considered previously, it is worthwhile to also consider how ion relaxation influences various vector fields such as the actual fluid velocity $\mathbf{v}(\mathbf{r})$ in the vicinity of a sedimenting or electrophoresing particle. First of all, consider the velocity field $\mathbf{v}_0(\mathbf{r})$ of a sedimenting 20-bp DNA fragment in the absence of ion relaxation translating with velocity $\mathbf{u}_0$ in a direction parallel to the cylinder axis. The velocity field is shown in Fig. 8 for a plane of fluid that passes through the cylinder axis. The reference frame is chosen to be stationary relative to the laboratory, and the instantaneous velocity is downward in the figure. The actual value of $\mathbf{u}_0$ is unimportant provided its magnitude is sufficiently small to insure low Reynolds number flow conditions (Happel and Brenner, 1963). A value of 5×10^{-4} cm/s is used here as a reference value. We shall also assume stick boundary con-

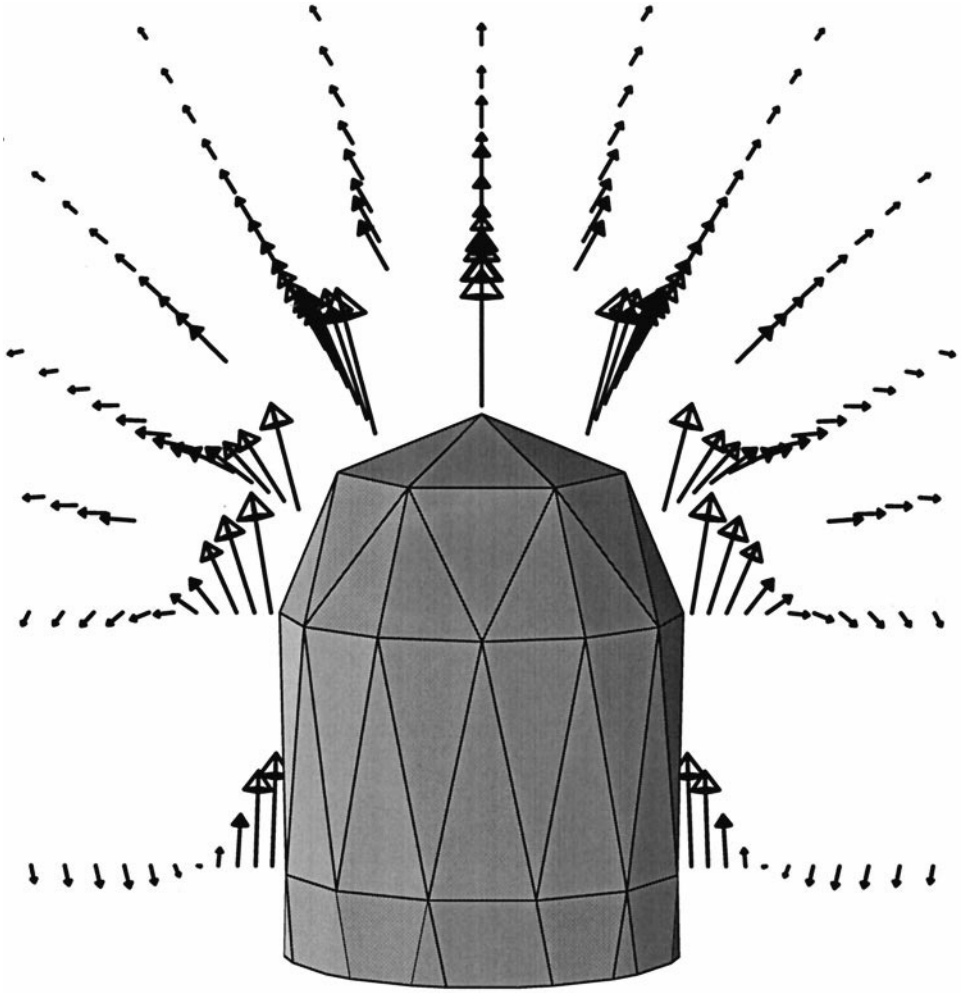

FIGURE 13 Close-up view of the relaxation field for electrophoresis of 20-bp DNA in 0.11 M KCl. Similar to Fig. 12, but the relaxation field near the tip of the polyion has been magnified. The relative magnitude of the vectors at the polyion surface are the same as in Fig. 8; however, the absolute value of the surface vectors in this figure are 18% as large as those in Fig. 8.

ditions hold, which means $\mathbf{v}_0(\mathbf{r}) = \mathbf{u}_0$ for points $\mathbf{r}$ on the polyion surface. Also, the upper and lower portions of the capped cylinder models have been cut away in Fig. 8 to illustrate more clearly the flow pattern near the particle. These fields are generated numerically by a BE procedure described elsewhere (Allison, 1996). As can be seen, the velocity field falls off rather slowly with distance away from the particle, and the pattern is similar to the velocity field profile for a sphere (Stigter, 1980). For a sedimenting DNA with ion relaxation, the flow pattern is similar to that shown in Fig. 8. If we compare two DNA fragments subject to exactly the same centrifugal force but one with ion relaxation accounted for and the other with ion relaxation ignored, the sedimentation velocity of the fragment with ion relaxation included would be smaller. In our reference example, ion relaxation would reduce the sedimentation velocity from 5.00×10^{-4} to 4.68×10^{-4} cm/s in 0.03 M KCl and from 5.00×10^{-4} to 4.86×10^{-4} in 0.11 M KCl. This is due to the fact that the sedimenting fragment in the absence of ion relaxation is entirely equivalent to the sedimentation of an uncharged particle of the same size and shape. The charged particle with ion relaxation sediments more slowly as it experiences additional frictional drag brought about by the tendency of the atmosphere to lag behind the polyion itself. In what follows, the difference velocity field, or relaxation field, shall be plotted:

$$\delta\mathbf{v}(r) = \mathbf{v}(r) - \mathbf{v}_0(r), \tag{5}$$

where the 0 subscript refers to the analogous unrelaxed case. The difference fields for sedimentation are shown in Figs. 9 (0.03 M) and 10 (0.11 M KCl). At the particle surface, the difference fields point in a direction opposite to that shown in Fig. 8, which is due to the fact $\mathbf{u}$ is in the same direction as $\mathbf{u}_0$ but smaller in magnitude. For our reference example, the magnitude of $\delta\mathbf{v}$ is 0.32×10^{-4} and 0.14×10^{-4} cm/s at 0.03 and 0.11 M KCl, respectively. Thus, the absolute magnitude of the vectors at the polyion surface are 6.4% (Fig. 9) and 2.8% (Fig. 10) as large as those of the surface vectors in Fig. 8. Comparing the relaxation field plots with the Stokes field plot of Fig. 8, it is clear that the relaxation fields fall off more quickly with distance and that they also exhibit a substantial salt dependence. At high salt, the relaxation field falls off more rapidly with distance than at low salt. Figs. 11 and 12 show the corresponding relaxation fields for steady-state electrophoresis at 0.03 and 0.11 M

KCl, respectively. The DNA fragment is placed in an electric field of 1 V/cm (directed in the direction of $\delta\mathbf{v}$ at the polyion surface). In the absence of relaxation, the DNA translates along the long axis under steady-state conditions with a velocity of 5×10^{-4} cm/s. Ion relaxation reduces these velocities to 3.60×10^{-4} and 4.10×10^{-4} cm/s at 0.03 and 0.11 M KCl, respectively. Thus, the magnitude of the relaxation fields at the polyion surface in Figs. 11 and 12 are 28% and 18% as large as the magnitude of the Stokes velocity field at the polyion surface (Fig. 8). Although similar to the previous figures for sedimentation, the corresponding relaxation fields for electrophoresis fall off even more quickly with distance. Fig. 13 is similar to Fig. 12 but represents a blow-up of the relaxation velocity field in the vicinity of one end of the polyion. Also note in Fig. 13 that there is a small reversal of the relaxation field at some distance from the polyion surface. Keep in mind, however, that these relaxation velocities are not actual velocities but difference velocities according to Eq. 5. Consequently, the actual velocity field does not reverse itself. At 0.11 M, the fall-off in the relaxation field appears sufficiently rapid that thin double layer theories (O'Brien, 1983; Solomentsev et al., 1993) may actually be appropriate.

Current fluxes

Finally, we would like to examine current fluxes around 20-bp DNA. Shown in Fig. 14 is the difference current, $\mathbf{j}_d = \mathbf{j}_+ - \mathbf{j}_-$ at 0.002 M KCl in the case of steady-state electrophoresis. The frame of reference is chosen to be stationary relative to the polyion. In the lab frame, the DNA moves downward in the figure and the electric field points upward. Near the DNA, the difference current is dominated by the flux of counterions $\mathbf{j}_+$, and it is worth considering which term(s) on the right side of Eq. 3 dominate the transport process. It cannot be the convective term as in a frame of reference stationary with respect to the polyion, $n_\alpha\mathbf{v}$ would vanish at the polyion surface and reach some plateau value at some distance. This, however, is inconsistent with Fig. 14. The direct force term (third term on the right side of Eq. 3) is expected to be dominated by the + ions interacting with the **e** field and be greatest near the polyion surface. This, however, would yield a flow pattern directed upward (along **e**) in Fig. 14. Close to the sides of the DNA, the flow pattern is seen to be just the opposite of this. This leaves the second term, which corresponds to diffusion against a concentration gradient. From Fig. 3, we know that there is an excess of counterions at the top end of the fragment and a deficiency at the other end. Also, the counterion concentration will be greatest near the polyion surface. Thus, the flow pattern near the sides of the DNA in Fig. 14 is entirely consistent with what one would expect if Eq. 3 were dominated by the diffusion term. Shown in Fig. 15 is exactly the same vector field but at the higher salt concentration of 0.11 M. It is worth noting that the sign of $\mathbf{j}_d$ close to the sides of DNA is reversed relative to Fig. 14 despite the fact the **e** values are the same in the two cases and the **u** values are at least in the same direction. Based on our previous discussion, it is clear that the direct force term in Eq. 3 dominates the ion flux at 0.11 M salt whereas the diffusive term dominates at low salt. Similar studies over a range of salt concentrations reveal that the general flow pattern seen in Fig. 15 occurs except at very low salt (less than ~0.005 M monovalent salt).

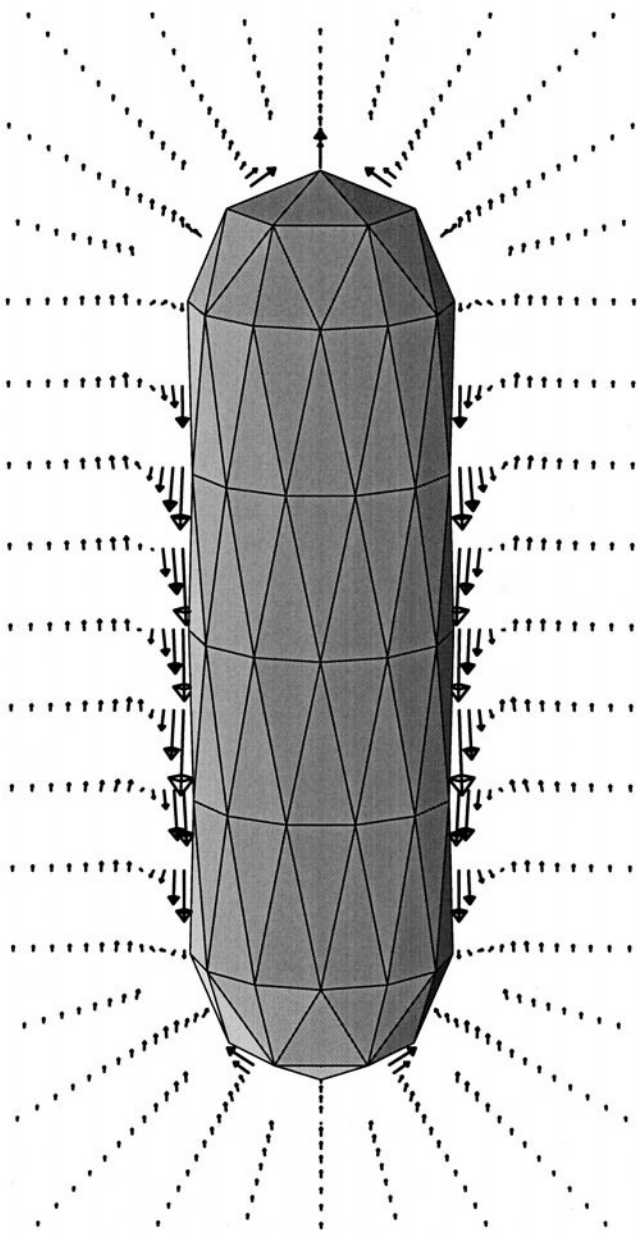

FIGURE 14 $\mathbf{j}_d$ for the electrophoresis of 20-bp DNA in 0.002 M KCl. The electric field is directed upward in a direction opposing the direction of $\mathbf{j}_d$ seen in the figure close to the sides of the polyion. The DNA translates downward. The reference frame is stationary with respect to the DNA.

We can offer the following simple physical interpretation of this phenomenon. In general, a DNA fragment undergoing steady-state electrophoresis and moving parallel to the long axis of the molecule will have one end that is rich in

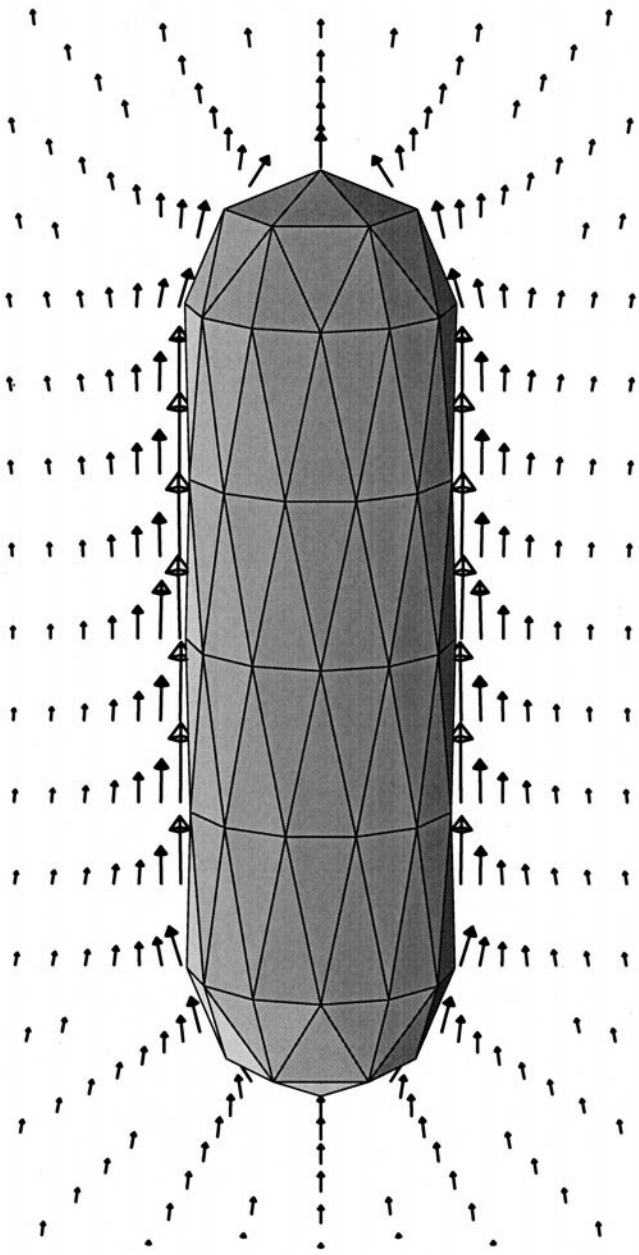

FIGURE 15 $\mathbf{j}_d$ for the electrophoresis of 20-bp DNA in 0.11 M KCl. Similar to Fig. 14, but at a higher salt concentration.

counterions and one end that is poor in counterions. At low salt, the primary source of counterions for the poor end is diffusion, against a concentration gradient, of counterions from the rich end (and sides) to the poor end. At high salt, the primary source of counterions for the poor end is the bulk solution where they are now present in abundance. As the + ions in the bulk solution tend to move in the general direction of e, this is reflected in the flow field for $\mathbf{j}_d$.

CONCLUSIONS

The primary objective of this work has been the graphic illustration of the phenomenon of ion relaxation in the transport of short DNA fragments. Contour plots of counterion and/or charge density have been presented for both 20- and 40-bp fragments at 0.03 and 0.11 M monovalent salt (KCl). Ion relaxation extends out distances of order κ^{-1} from the ends of the fragment for the DNA translating parallel to its cylinder axis. The relaxation effect is similar for sedimentation and electrophoresis, but there are differences. In addition, vector plots of the Stokes field and the relaxation velocity field are presented for both sedimentation and electrophoresis of 20-bp DNA. The relaxation effect falls off rapidly with distance, and this fall-off is more rapid at higher salt. These results are qualitatively similar to an earlier study of charged spheres (Stigter, 1980). Finally, the charge current flux around the 20-bp fragment is examined at 0.002 and 0.11 M KCl. At the lower salt concentration, the charge flux is dominated by diffusion against a concentration gradient, but at the higher salt concentration, the dominant term involves the force on the counterions by the external electric field. The charge current flux plays a central role in the theory of conductance of polyelectrolytes (Stigter, 1979), and the results presented here will be expanded upon in future work.

This work was supported in part by National Science Foundation grants MCB-9807541 (to S.A. Allison) and MCB-9807550 (to T.M. Laue).

REFERENCES

Allison, S. A. 1996. Modeling the electrophoresis of rigid polyions: inclusion of ion relaxation. *Macromolecules*. 29:7391–7401.

Allison, S. A. 1998. The primary electroviscous effect of rigid polyions of arbitrary shape and charge distribution. *Macromolecules*. 31: 4464–4474.

Allison, S. A., and S. Mazur. 1998. Modeling the free solution electrophoretic mobility of short DNA fragments. *Biopolymers*. 46:359–373.

Allison, S. A., M. Potter, and J. A. McCammon. 1997. Modeling the electrophoresis of lysozyme. II. Inclusion of ion relaxation. *Biophys. J.* 73:133–140.

Booth, F. 1950a. The cataphoresis of spherical, solid non-conducting particles in a symmetric electrolyte. *Proc. R. Soc. London*. 203A: 514–533.

Booth, F. 1950b. The electroviscous effect for suspensions of solid spherical particles. *Proc. R. Soc. London.* 203A:533–551.

Booth, F. 1954. Sedimentation potential and velocity of solid spherical particles. *J. Chem. Phys.* 22:1956–1968.

Diekmann, S., W. Hillen, B. Morgeneyer, R. D. Wells, and D. Porschke. 1982. Orientation relaxation of DNA restriction fragments and the internal mobility of the double helix. *Biophys. Chem.* 15:263–270.

Elias, J. G., and D. Eden. 1981. Transient electric birefringence study of the persistence length and electric polarizability of restriction fragments of DNA. *Macromolecules.* 14:410–419.

Fixman, M., and S. Jagannathan. 1981. Electrical and convective polarization of cylindrical macroions. *J. Chem. Phys.* 75:4048–4059.

deGroot, S. R., P. Mazur, and J. T. G. Overbeek. 1952. Nonequilibrium thermodynamics of the sedimentation potential and electrophoresis. *J. Chem. Phys.* 20:1825–1829.

Hagerman, P. J. 1981. Investigation of the flexibility of DNA using transient electric birefringence. *Biopolymers*. 20:1503–1535.

Happel, J., and H. Brenner. 1963. Low Reynolds Number Hydrodynamics. Martinus Nijhoff Publishers, The Hague.

Holst, M. J., and F. Saied. 1995. Numerical solution of the nonlinear Poisson-Boltzmann equation: developing more robust and efficient methods. *J. Comp. Chem.* 16:337–364.

Laue, T. M., T. M. Ridgeway, J. O. Wooll, H. K. Shepard, T. P. Moody, T. J. Wilson, J. B. Chaires, and D. A. Stevenson. 1996. Insights from a new analytical electrophoresis apparatus. *J. Pharmacol. Sci.* 85: 1331–1335.

McQuarrie, D. A. 1976. Statistical Mechanics. Harper and Row, Publishers, New York.

O'Brien, R. W. 1983. The solution of the electrokinetic equations for colloidal particles with thin double layers. *J. Colloid Interfac. Sci.* 92:204–216.

O'Brien, R. W., and L. R. White. 1978. Electrophoretic mobility of a spherical colloidal particle. *J. Chem. Soc. Faraday II.* 74:1607–1626.

Porschke, D. 1994. DNA double helices with positive electric dichroism and permanent dipole moments: non-symmetric charge distributions and "frozen" configurations. *Biophys. Chem.* 49. 127–139.

Sherwood, J. D. 1980. The primary electroviscous effect in a suspension of spheres. *J. Fluid Mech.* 101:609–629.

Sherwood, J. D. 1981. The primary electroviscous effect in a suspension of rods. *J. Fluid Mech.* 111:347–366.

Solomentsev, Y. E., Y. Pawar, and J. L. Anderson. 1993. Electrophoretic mobility of nonuniformly charged spherical particles with polarization of the double layer. *J. Colloid Interfac. Sci.* 158:1–9.

Stellwagen, N. C. 1981. Electric birefringence of restriction enzyme fragments of DNA: optical factor and electric polarizability as a function of molecular weight. *Biopolymers*. 20:399–424.

Stellwagen, N. C., C. Gelfi, and P. G. Righetti. 1997. The free solution mobility of DNA. *Biopolymers*. 42:687–703.

Stigter, D. 1978a. Electrophoresis of highly charged colloidal cylinders in univalent salt solutions. I. Mobility in transverse field. *J. Phys. Chem.* 82:1417–1423.

Stigter, D. 1978b. Electrophoresis of highly charged colloidal cylinders in univalent salt solution. II. Random orientation in external field and application to polyelectrolytes. *J. Phys. Chem.* 82:1424–1429.

Stigter, D. 1979. Theory of conductance of colloidal electrolytes in univalent salt solutions. *J. Phys. Chem.* 83:1663–1670.

Stigter, D. 1980. Sedimentation of highly charged colloidal spheres. *J. Phys. Chem.* 84:2758–2762.

Tinoco, I., and K. Yamaoka. 1959. The reversing pulse technique in electric birefringence. *J. Phys. Chem.* 63:423–427.

Wiersema, P. H., A. L. Loeb, and J. T. G. Overbeek. 1966. Calculation of the electrophoretic mobility of a spherical colloid particle. *J. Colloid Interfac. Sci.* 22:78–99.

Wooll, J. O. 1994. Investigation of $pd(A)_{20} \cdot pd(T)_{20}$ in the analytical electrophoresis apparatus. Ph.D. Thesis. University of New Hampshire, Durham, NH. Table 3, page 51.

Zhou, H.-X. 1994. Macromolecular electrostatic energy within the nonlinear Poisson-Boltzmann equation. *J. Chem. Phys.* 100:3152–3162.